GeV–TeV Cosmic-Ray Leptons in the Solar System from the Bow Shock Wind Nebula of the Nearest Millisecond Pulsar J0437–4715

A. M. Bykov[1,2,3] , A. E. Petrov[1] , A. M. Krassilchtchikov[1] , K. P. Levenfish[1] , S. M. Osipov[1] , and G. G. Pavlov[4]
[1] Ioffe Institute, 26 Politehnicheskaya, St. Petersburg, 194021, Russia; byk@astro.ioffe.ru
[2] Peter the Great St. Petersburg Polytechnic University, St. Petersburg, 195251, Russia
[3] International Space Science Institute, Hallerstrasse 6, 3012 Bern, Switzerland
[4] Department of Astronomy and Astrophysics, Pennsylvania State University, PA 16802, USA

Abstract

We consider the acceleration of leptons up to GeV–TeV energies in the bow shock wind nebula of PSR J0437–4715 and their subsequent diffusion through the interstellar magnetic fields. The leptons accelerated at the pulsar wind termination surface are injected into re-acceleration in colliding shock flows. Modeled spectra of synchrotron emission from the accelerated electrons and positrons are consistent with the far-ultraviolet and X-ray observations of the nebula carried out with the *Hubble Space Telescope* and *Chandra X-ray Observatory*. These observations are employed to constrain the absolute fluxes of relativistic leptons, which are escaping from the nebula and eventually reaching the solar system after energy-dependent diffusion through the local interstellar medium accompanied by synchrotron and Compton losses. It is shown that accelerated leptons from the nebula of PSR J0437–4715 can be responsible both for the enhancement of the positron fraction above a few GeV detected by *PAMELA* and *AMS-02* spectrometers and for the TeV range lepton fluxes observed with *H.E.S.S.*, *VERITAS*, *Fermi*, *CALET*, and *DAMPE*.

Key words: acceleration of particles – cosmic rays – pulsars: individual (PSR J0437–4715) – shock waves

1. Introduction

Recent precise in-orbit measurements of cosmic-ray (CR) spectra in the GeV–TeV range performed by *PAMELA*, *AMS-02*, *H.E.S.S.*, *VERITAS*, *DAMPE*, and *CALET* have revealed a non-trivial structure of spectra of accelerated positrons and electrons (Aharonian et al. 2008, 2009; Abdo et al. 2009; Adriani et al. 2009, 2018; Ackermann et al. 2012; Accardo et al. 2014; Aguilar et al. 2014, 2019; DAMPE Collaboration 2017; Archer et al. 2018). In particular, Aguilar et al. (2019) have conducted precise flux measurements of CR positrons at energies up to 1 TeV and concluded that the CR positron flux in this energy regime can be represented as a sum of two components: one produced by inelastic collisions of CR nuclei with the interstellar gas and dominating at low energies, and the other originating from a yet-unknown source and dominating at high energies up to about 800 GeV. The second component shows a complex spectral behavior with a significant excess over the low-energy flux, which is prominent from about 25 GeV and then approximately follows a power law up to 250–300 GeV. Inelastic interactions of the energetic hadronic component of galactic CRs with the nuclei of the local interstellar medium (ISM) produce positrons as well as antiprotons and other secondary nuclei (see, e.g., Moskalenko & Strong 1998; Vladimirov et al. 2012, and references therein). However, it seems difficult to understand the origin of the growth of the positron fraction in the CR leptons above 10 GeV due to the CR nuclei interactions (see, e.g., Aguilar et al. 2019).

The two alternatives to the origin of excess positrons as secondary CRs are the annihilation or decay of dark matter particles (e.g., Silk & Srednicki 1984; Bertone et al. 2005; Bergström et al. 2008) and the presence of local sources of accelerated electrons and positrons, which are believed to come from energetic pulsars and supernova remnants (Atoyan et al. 1995; Hooper et al. 2009; Malyshev et al. 2009; Yüksel et al.

2009; Blasi & Amato 2011; Kisaka & Kawanaka 2012; Profumo 2012).

Pair acceleration by pulsars (both in the magnetosphere and at the termination shock) was discussed as a possible source of the observed positron excess above a few GeV. Malyshev et al. (2009) noted that acceleration at the pulsar wind (PW) termination shock is required to produce the multi-GeV positrons consistent with *PAMELA* data.

Büsching et al. (2008) and Venter et al. (2015) showed that pair cascades from the magnetospheres of millisecond pulsars without wind nebulae could only modestly contribute to the CR lepton fluxes near the Earth at a few tens of GeV, and that this component would cut off at higher energies. However, they pointed out that strong intrabinary shocks in redback and black-widow-type pulsars may allow them to contribute to 10–40 TeV CR fluxes near the Earth. As the propagation distance of the accelerated $e^{\pm}$ pairs would decrease with energy, at higher energies their spectrum should become bump-like (e.g., Cholis et al. 2018). In any case, once observed with a significant confidence, the lepton spectra at TeV energies favor a major contribution from only one or few local sources; otherwise, the bump would be smoothed away.

Because of the young estimated pulsar age of about 11 kyr, the nearby Vela PW nebulae could contribute to the observed lepton fluxes only if the diffusion coefficient for the particle energies of interest were about 10^{30} cm^2 s^{-1}. This value is somewhat large for the energy range 10–100 GeV, both for transport inside a supernova remnant and for the local ISM, thus making a substantial contribution from this pulsar to the observed lepton fluxes at 10–100 GeV unlikely. Above 100 GeV some possible contribution from the Vela-X pulsar wind nebula (PWN) was discussed (see, e.g., Della Torre et al. 2015). The nearby middle-aged pulsars Geminga and PSR B0656+14 could be potential sources of accelerated leptons (see, e.g., Fang et al. 2018; Profumo et al. 2018; Tang

& Piran 2019). The nearby middle-aged PSR B1055–52 may have a weak X-ray PWN (Posselt et al. 2015). The source has a spindown power similar to that of PSR J0437–4715 (which we will discuss in detail here), but it is apparently farther away (Mignani et al. 2010).

The High-Altitude Water Cherenkov Observatory (HAWC) reported a detection of extended TeV gamma-ray emission from Geminga and PSR B0656+14 (Abeysekara et al. 2017). Analyzing the observed gamma-ray emission profiles with a single-zone diffusion model, the HAWC team concluded that the CR diffusion in the source vicinities is too slow for these pulsars to be responsible for the positron excess observed by *PAMELA* and *AMS-02*. However, two-zone models with slow diffusion in the inner zone of about 40 pc around the nebulae and fast diffusion in the local ISM (Fang et al. 2018; Profumo et al. 2018; Tang & Piran 2019) can explain, under some conditions, both the TeV emission profiles and the observed positron excess. The diffusion coefficient in the inner zone around a PWN (the "TeV halo") can be strongly suppressed compared to the background ISM due to nonlinear effects of turbulence driven by CRs escaping the source (see, e.g., Malkov et al. 2013; Evoli et al. 2018). This requires a high pulsar spindown power and its efficient conversion to CR pressure. To fit the *AMS-02* data, Fang et al. (2018) had to assume at least 75% efficiency of Geminga's spindown power conversion into energetic CRs. Based on a two-zone model, Tang & Piran (2019) concluded that the Geminga PWN could significantly contribute to the observed positron excess above 300 GeV, while another source is needed to provide the positrons between 10 and 300 GeV. Hooper & Linden (2018) performed a stacked analysis of 24 old recycled millisecond pulsars within the field of view of the HAWC observatory. They found evidence of the presence of TeV halos around these millisecond pulsars on the 2.6–3.1σ level.

An analysis presented by López-Coto et al. (2018b) suggested that an undiscovered pulsar with the spindown power $\sim 10^{33-34}$ erg s^{-1} should exist in the 80 pc vicinity of the solar system to explain the observed TeV spectral feature, assuming a very low local CR diffusion coefficient $\sim 10^{26} \times (E/10 \text{ GeV})^{0.33}$ cm^2 s^{-1}. On the other hand, Recchia et al. (2018) pointed out that because the measured growth of the positron fraction above a few GeV saturates at a level well below 0.5, and may even drop down above $\sim$ 400–500 GeV (though the *AMS-02* data have rather large statistical errors at these energies), the local sources of TeV leptons should not produce positrons and electrons in equal amounts. Recchia et al. (2018) claimed that this would rule out PWs as main sources of TeV range leptons, and proposed instead the presence of a single local fading source of TeV range electrons, which might be an old supernova remnant or another object. Hence, to constrain the source models, one would need to carry out high-precision measurements of the positron fraction at 0.5–2 TeV energies where the flux suppression (a spectral break feature) was revealed by *DAMPE* and *CALET*.

When energetic pulsars powering PWNe move through the ISM with supersonic velocities, they form bow shocks, which are often discovered via their Hα emission (see, e.g., Brownsberger & Romani 2014, and references therein). While PWNe and bow shocks are rare among the old rotation-powered millisecond pulsars (e.g., Bogdanov 2017), they have been studied in some detail for a dozen of young and middle-aged pulsars (Kargaltsev et al. 2017). Such bow shock pulsar wind nebulae (BSPWNe) are considered among main possible contributors to the positron population of the Galaxy (Blasi & Amato 2011; Bykov et al. 2017). Contrary to the slowly moving PWNe without bow shocks, BSPWNe can be the sites of a specific efficient acceleration of particles in the colliding shock flow (CSF) zone between the PW termination shock (or more generally, termination surface (TS); see Arons 2012) and the bow shock (Bykov et al. 2017). Such acceleration is likely the cause for the hard spectra of synchrotron X-rays observed in a number of BSPWNe (e.g., Geminga, see Posselt et al. 2017). The CR lepton spectrum in such BSPWNe probably consists of two components, one of them is due to $e^{\pm}$ pairs accelerated at the TS, and the other is formed in the CSF region.

The particle spectrum $f(E) \propto E^{-s}$, $s \sim 2.1$–2.3, formed in the vicinity of the PWN TS, can naturally account for the X-ray spectra of the Crab Nebula (see, e.g., Arons 2012) which has no bow shock, as well as some other Crab-like objects. However, it cannot explain the hard photon spectra of synchrotron X-rays detected from BSPWNe, namely, the hard X-ray photon indices $\Gamma \sim 1$ of the lateral tails of the Geminga PWN (Posselt et al. 2017) and of the inner region of the Vela PWN (Kargaltsev & Pavlov 2008). To explain these spectra, a second component with $s \sim 1$ at energies up to $E \sim 100$ TeV is required.

It was shown by Bykov et al. (2017) that starting at some high enough energy, the $e^{\pm}$ pairs accelerated at the TS, as well as electrons and protons accelerated at the bow shock, are injected into the acceleration in the CSF, where they form a power-law spectrum with $s < 2$ in some energy range. This can naturally explain the hard component of X-ray emission revealed in *Chandra* observations of a number of BSPWNe. It is important to note that the acceleration mechanism operating in CSFs transfers the available wind flow energy upward in the spectrum, i.e., to the $e^{\pm}$ pairs of the maximal energies that satisfy the condition of particle confinement in the acceleration region. This substantially increases the efficiency of transfer of the pulsar spindown power to the high-energy pairs. In Figure 1 it is shown that the CRs accelerated in the CSFs provide the hard spectrum component between a few hundred GeV and a few TeV. The power-law component at lower and higher energies is due to CR acceleration at the TS.

Accelerated particles from nearby BSPWNe can reach the solar system and are likely to contribute to the locally measured spectra of galactic cosmic ray (GCR) leptons. Below we discuss a model of particle acceleration in the BSPWN of the nearest millisecond pulsar PSR J0437–4715 and show that it can be the long-sought single source of the 10–800 GeV positron excess. The CR leptons accelerated in the source can contribute also to the lepton spectrum at TeV energies measured in the solar system, where the CR lepton flux suppression (spectral break) was observed by both *CALET* and *DAMPE* experiments (Adriani et al. 2018). The X-ray emission spectra observed from PSR J0437–4715 nebula are used to calibrate the absolute lepton fluxes from this source.

2. Modeling of Particle Acceleration in the Nebula of PSR J0437–4715

The nebula of the old millisecond pulsar PSR J0437–4715 was studied in the optical, far-ultraviolet (FUV), and X-ray bands with the *Hubble Space Telescope* and *Chandra X-ray Observatory* by Rangelov et al. (2016). PSR J0437–4715 is
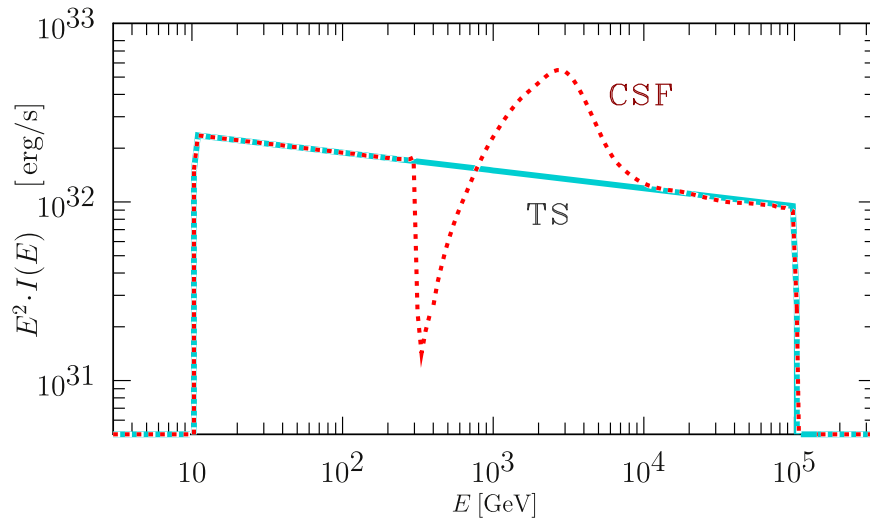
Figure 1. Modeled spectrum of cosmic-ray leptons escaping the nebula of PSR J0437–4715 both through the tail and bow shock regions. The spectra formed at the termination surface (TS) and in the colliding shock flow (CSF) are shown. The power carried away by the CR particles leaving the modeled bow shock nebula is about 30% of the estimated $\dot{E}$. Here $I(E) = \int J(E)d\Omega$ is the direction-integrated spectral flux of the accelerated leptons.

located at a precisely measured distance of 156.79 ± 0.25 pc (Reardon et al. 2016) in a binary system with a measured parallax. The transverse velocity of the system is ≈ 104 km s^{-1}. The maximal realistic spindown power of the pulsar[5] corrected for the Shklovskii effect is $\dot{E} \sim 6 \times 10^{33}$ erg s^{-1}, the number density of the ambient ISM derived from observations in the Hα band is about 0.2 cm^{-3} (see, e.g., Brownsberger & Romani 2014). The faint extended X-ray emission detected in the $5''$ vicinity of the pulsar by Rangelov et al. (2016) is associated with the PWN, whose X-ray luminosity $L_X \sim 3 \times 10^{28}$ erg s^{-1} and the photon index $\Gamma = 1.8 \pm 0.4$. The poorly constrained photon index allows both hard, $s \sim 1.5$, and soft, $s \sim 3$, indices of synchrotron radiating $e^{\pm}$ pairs in the multi-TeV energy range. FUV imaging revealed a bow shock structure with a $10''$ apex coinciding with the Hα bow shock earlier observed by Brownsberger & Romani (2014). The unabsorbed $1250–2000$ Å luminosity of the bow shock $L_{\rm FUV} \sim 5 \times 10^{28}$ erg s^{-1} is an order of magnitude higher than its Hα luminosity (Rangelov et al. 2016). The observed FUV bow shock radiation can be produced by both the heated interstellar gas emitting spectral lines such as C IV 1549 Å, O IV 1403 Å, Si IV 1397 Å, C II 1335 Å, He II 1640 Å, and continuum synchrotron radiation of electrons and positrons of the PW. To disentangle this contributions, FUV spectroscopy of the nebula is required.

Based on observations of young pulsars, such as the Crab pulsar, it is reasonable to assume that a nonthermal distribution of $e^{\pm}$ pairs of $f(E) \propto E^{-s}$, $s \sim 2.1$–2.3, which is responsible for the observed X-ray nebula, forms in the vicinity of the wind TS of PSR J0437–4715. An important issue is the composition of the PW: in addition to $e^{\pm}$ pairs, the wind may contain a minor (by number density) but energetically significant ion component, which may have important implications for modeling of the ultra-high-energy CRs (see, e.g., Kotera et al. 2015; Lemoine et al. 2015). Particle-in-cell simulation of relativistic shocks in electron–positron–proton plasmas with $m_p/m_e = 100$ (Amato & Arons 2006) demonstrated that the

acceleration efficiency and the spectra of the accelerated particles depend on the plasma composition upstream of the shock. 1D simulations revealed that if a sizeable fraction of the incoming energy flux is contained in protons, the nonthermal distribution of $e^{\pm}$ pairs would form in the shock downstream with different spectral shapes of electrons and positrons. Namely, the positron spectra would be characterized by harder power-law spectral indices, but lower cutoff energies than those of the accelerated electrons. In this case the positron fraction may vary with energy and be both above and below 0.5 in different energy ranges. For the case of PSR J0437–4715 we assumed the dominance of electrons in the spectral cutoff regime. As reliable models of PWs including the ion component are not available as of yet, we considered parameterized distributions of accelerated positrons and electrons at the TS of the wind of PSR J0437–4715. This parameterization assumed equal amounts of electrons and positrons in the TS spectrum shown in Figure 1, with an electron-dominated high-energy end.

We used the Monte Carlo modeling to simulate particle transport after leaving the PW TS, where a power-law particle spectrum is thought to be produced (see the curve labeled "TS" in Figure 1). The minimal Lorentz factor of the leptons accelerated at the TS was assumed to be about the Lorentz factor of the cold PW of PSR J0437–4715. The actual low-energy cutoff might be rather smooth. However, we do not discuss here the CR spectrum below 10 GeV affected by the solar wind modulation. Thus we simply assume a sharp low-energy cutoff at ~ 10 GeV. The maximal energy is parameterized as a fraction of the total magnetospheric potential $e\sqrt{\dot{E}/c}$ (see, e.g., Arons 2012). The energy cp_* at the peak of the lepton component re-accelerated at the CSF (the dotted red line labeled "CSF" in Figure 1) is determined by the diffusion coefficient inside of the bow-shock PWN $D(p_*)$. This energy can be estimated from $D(p_*) \approx u_{\rm psr} R_{\rm sh}$, where $u_{\rm psr}$ is the proper velocity of the pulsar and $R_{\rm sh}$ is the size of the CSF accelerating region which is about the apparent bow shock apex size (for details, see Bykov et al. 2017).

In the Monte Carlo simulation the injected TS spectrum had a low-energy cutoff at the Lorenz factor

---

[5] This value corresponds to a stiff equation of state, which allows the moment of inertia of a 1.44 $M_\odot$ neutron star to reach 2×10^{45} g cm^2.
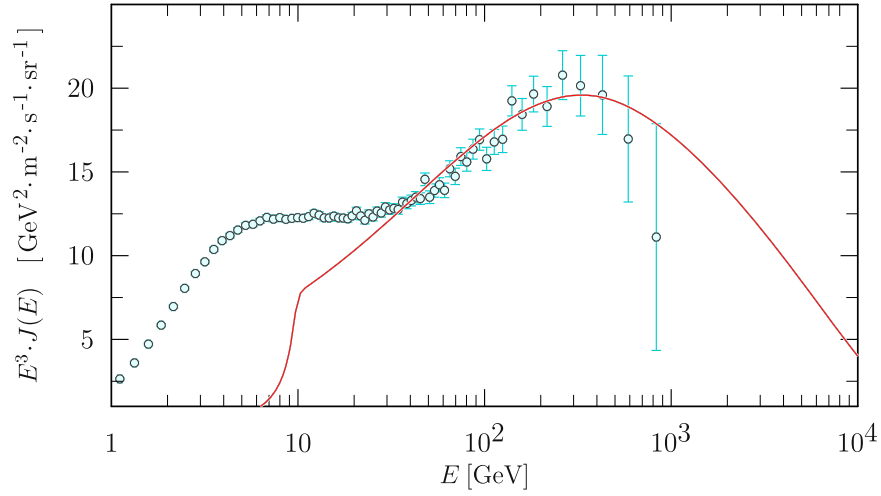
Figure 2. Model spectrum of cosmic-ray positrons (red) in the solar system produced by the nebula of PSR J0437–4715 after diffusion through the local interstellar medium with account of synchrotron/Compton energy losses is shown together with the observed spectrum (blue; Aguilar et al. 2019). The considered diffusion is anisotropic, with the parallel and transverse diffusion coefficients $D_\parallel = 2 \times 10^{27}(E/1\,\mathrm{GeV})^{1/3}$ cm^2 s^{-1} and $D_\perp = 0.03D_\parallel$, respectively.

$\gamma = \gamma_0 \sim (2 - 8) \times 10^5$. Particles with lower energies are not involved in the CSFs, they are advected to the tail of the nebula by the PW flow.

The escaping particle flux $J_{\mathrm{calc}}(E)$ and the energy flux $\Phi_{\mathrm{calc}}(E)$ carried by the particles escaping the source were calculated within a Monte Carlo simulation (see Figure 1). The flux of escaping particles was considered as the source term in the transport equation, which described the CR lepton diffusion in the ISM with synchrotron and Compton losses. This equation was solved to obtain the contribution of the BSPWN of PSR J0437–4715 to the CR lepton flux observed near the Earth.

The Monte Carlo technique allows one to calculate the particle distribution function f_{calc} at a discrete spatial grid as well as the fluxes J_{calc}, Φ_{calc} through a given surface surrounding the source. These values are further rescaled to match the observed fluxes. Namely, using the observed PWN X-ray flux, $F_{\mathrm{obs}} = 10^{-14}$ erg cm^{-2} s^{-1}, and the model flux value $F_{\mathrm{calc}} = \int I_\nu^{\mathrm{calc}} \cos\theta d\Omega d\nu$, one can rescale the model particle flux J:

$$J = \frac{F_{\mathrm{obs}}}{F_{\mathrm{calc}}} J_{\mathrm{calc}}. \qquad (1)$$

The value F_{calc} is obtained via a standard integration over the solid angle Ω and frequency ν of I_ν^{calc}, the synchrotron emission intensity, which is calculated along a given line of sight using the simulated local particle spectra f_{calc} and standard formulae for the synchrotron emissivity in the chaotic magnetic field (Crusius & Schlickeiser 1986).

To model the observed fluxes, at the first step the particle distribution function is simulated in the entire volume of the modeled source and the source synchrotron emission is calculated. After calculation the flux F_{calc} from the PWN, particle, and energy fluxes through the source boundary are calculated. Finally, the transport equation with the source term determined by the spectrum of escaping CR leptons is solved. The model of particle transport from the source to the solar system includes anisotropic CR diffusion in the ISM and CR particle energy losses due to synchrotron and inverse Compton radiation. The inverse Compton losses are accounted for with the approximation of Moderski et al. (2005).

CR transport from nearby sources located at the distance comparable with the coherence length of the interstellar magnetic field (about 100 pc) can differ from the global CR diffusion in the Galaxy (see, e.g., Seta et al. 2018). In this study we employ anisotropic diffusion to consider the CR transport. This is because the CR particles at the energies of interest (below a few TeV) are highly magnetized; i.e., their gyroradii are much smaller than both their mean free paths and the coherence scale of the turbulent magnetic field L_{m}. In this case the diffusion coefficient across the local ordered magnetic field $D_\perp$ is much smaller than $D_\parallel$, which describes the parallel diffusion.

Detailed Monte Carlo simulations of CR transport in chaotic magnetic fields made by Casse et al. (2002) and Candia & Roulet (2004) show that in the case of Kolmogorov-type turbulence, which is supported by observations of interstellar magnetic fields at low rigidities $\rho = 2\pi\, r_g/L_{\mathrm{m}} < 1$, the diffusion coefficient $D_\parallel \propto \rho^{1/3}$, while the ratio $D_\perp/D_\parallel$ does not depend on the CR particle energy. Here $r_g = E/eB$ is the particle gyroradius, E and e are the particle energy and charge, B is the mean magnetic field. The condition $\rho < 1$ is well satisfied in the ISM with typical magnetic field $B_{\mathrm{ISM}} \sim 3$ μG and $L_{\mathrm{m}} \sim 10^2$ pc. The energy dependence $D_\parallel \propto \rho^{1/3}$ matches the inferred energy dependence of the global (average) CR diffusion coefficient in the Galaxy, $D \approx 3 \times 10^{28}(E/1\,\mathrm{GeV})^\delta$ cm^{2}s^{-1}, $\delta \sim 1/3$ (see, e.g., Strong et al. 2007). Global diffusion averaged over the galactic scales can be described as nearly isotropic diffusion, while the local diffusion at scales comparable to the coherence scale of the galactic magnetic field is highly anisotropic. Here we employed $D_\perp = 0.03D_\parallel$ in accordance with the results by Casse et al. (2002).

The direction of the local ordered ISM magnetic field—l, $b = 36°.2, 49°.0$ ($\pm 16°.0$)—was derived by Frisch et al. (2015) from observations of polarized starlight and from analysis of the *IBEX* Ribbon observations. In the CR production and transport modeling presented in Figures 2 and 3 the local ordered magnetic field $B_{\mathrm{ISM}} = 3.7$ μG was taken to be directed at $l = 52°$ $b = 49°$, which is consistent with Frisch et al. (2015) within the specified uncertainties.

The coefficient of parallel diffusion $D_\parallel(p)$ in the Local (super)Bubble is thought to be somewhat lower than the global
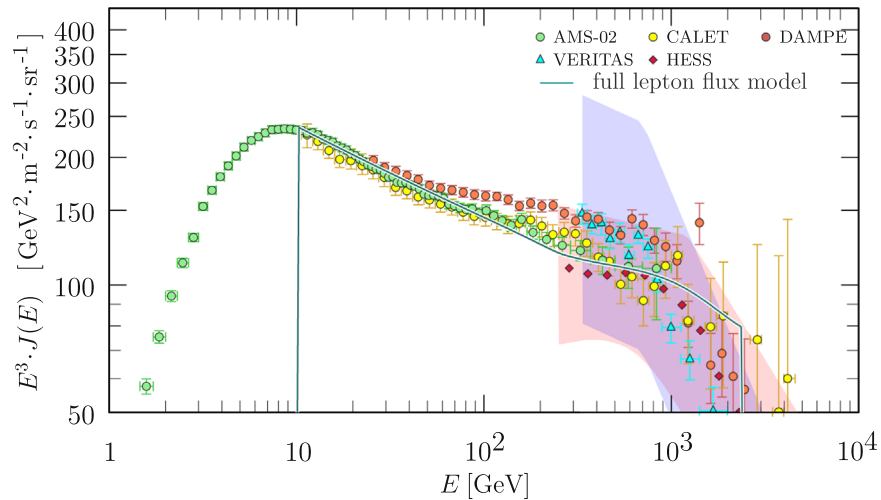
Figure 3. Model spectrum of CR leptons originating from the nebula of PSR J0437–4715 confronted with the data measured by *AMS-02*, *H.E.S.S.*, *DAMPE*, *VERITAS*, and *CALET* experiments (see Section 1). The pink and blue shaded regions indicate the systematic errors of *H.E.S.S.* and *VERITAS*, respectively.

average value referred above. Thus, in the anisotropic diffusion model, we adopt $D_\parallel(p) = 2 \times 10^{27}(E/1\,\text{GeV})^{1/3}\,\text{cm}^2\,\text{s}^{-1}$, which is consistent with that suggested by Yüksel et al. (2009), López-Coto et al. (2018a), and Tang & Piran (2019). It should be noted that satisfactory fits to the observed fluxes shown in Figures 2 and 3 can be obtained for a wide parameter space of the ordered field direction and the value of diffusion coefficient.

In Figure 3 a model spectrum of CR leptons in the solar system is shown, with the contribution from PSR J0437–4715 dominating at high energies. The blue curve shows the sum of the modeled lepton flux from PSR J0437–4715 with the contribution from other sources of CR leptons. The spectral shape of that contribution in the whole range from ∼10 GeV to few TeV is given by power-law models with indices 2.94 and 3.25 for positrons and electrons, respectively, matching the power-law fit of the low-energy (∼15–30 GeV) component of the total CR lepton spectrum of Aguilar et al. (2014). The lepton flux measurements made with *AMS-02*, *H.E.S.S.*, *VERITAS*, *DAMPE*, and *CALET* (see Aharonian et al. 2008; DAMPE Collaboration 2017; Adriani et al. 2018; Archer et al. 2018; Aguilar et al. 2019) are also shown in Figure 3. The region colored in pink indicates the systematic errors of *H.E.S.S.*,[6] while the region colored in blue is the same for *VERITAS*.

The positron fraction in the source spectrum in Figure 1 was assumed to be 0.5 to simulate the fluxes measured at the Earth's orbit, which are shown in Figure 2. If the positron fraction is different from this value in the source, then the fluxes can be scaled correspondingly. Moreover, the spectra of positrons and electrons may differ as well as their maximal momenta at the TS if the ions are energetically important in the PW according to the microscopic simulations of Amato & Arons (2006) discussed above. In this case, the CR lepton spectra in the flux suppression (spectral break) regime in Figure 3 provided by PSR J0437–4715 would be dominated by TeV regime electrons consistent with the *AMS-02* positron data by Aguilar et al. (2019). This important issue deserves further investigation via 3D particle-in-cell modeling with realistic electron-to-ion mass ratio. The flattening of the modeled total lepton

spectrum above 200 GeV in Figure 3 is due to CR acceleration in the CSFs behind the bow shock of PSR J0437–4715 (see the bump in Figure 1).

3. Summary

We have shown that the expected flux of the high-energy $e^\pm$ pairs from the bow shock nebula of PSR J0437–4715 can explain the enhanced $e^+/(e^- + e^+)$ ratio detected near the Earth with magnetic spectrometers *PAMELA* and *AMS-02*, from about 10 GeV up to 800 GeV, as well as the flux suppression (spectral break) in the TeV range found with *CALET* and *DAMPE*.

A distinctive feature of the suggested model is that the absolute fluxes of the leptons accelerated in the nebula of PSR J0437–4715 are derived from the model of its synchrotron emission. The model employs the assumptions about the structure of the plasma flows and the magnetic field strength in the nebula (of a few tens of μG) consistent with the recent numerical magnetohydrodynamic simulations by Barkov et al. (2019) and Olmi & Bucciantini (2019). Comparison of the model predictions with the optical, FUV, and X-ray observations of PSR J0437–4715 and its nebula (see Rangelov et al. 2016) allows us to estimate the absolute fluxes of CR leptons accelerated in the nebula. The model is also capable of reproducing the FUV and X-ray morphology of the BSPWN. In particular, the synchrotron emission of the accelerated $e^\pm$ pairs can explain the 1250–2000 Å FUV radiation of the bow shock region. This emphasizes the importance of FUV spectroscopy of this nebula to separate the contribution of the emission lines from the hot plasma in the bow shock downstream from the synchrotron continuum. Within the suggested model, only about 30% of the pulsar spindown power is required to be converted into accelerated $e^\pm$ pairs.

Although the model of CR lepton acceleration in PSR J0437–4715 described above allows one to reproduce the available observations of *PAMELA*, *AMS-02*, *DAMPE*, *CALET*, *H.E.S.S.*, and *VERITAS*, a significant contribution to the observed fluxes of accelerated leptons from some other nearby pulsars (Geminga, PSR B0656+14, PSR B1055–52) cannot be excluded.

---

[6] See https://www.mpi-hd.mpg.de/hfm/HESS/pages/home/som/2017/09/.

ORCID iDs

A. M. Bykov https://orcid.org/0000-0003-0037-2288
A. E. Petrov https://orcid.org/0000-0001-8356-9654
A. M. Krassilchtchikov https://orcid.org/0000-0001-7681-4316
K. P. Levenfish https://orcid.org/0000-0001-8063-0034
S. M. Osipov https://orcid.org/0000-0001-8806-0259
G. G. Pavlov https://orcid.org/0000-0002-7481-5259

References

Abdo, A. A., Ackermann, M., Ajello, M., et al. 2009, PhRvL, 102, 181101
Abeysekara, A. U., Albert, A., Alfaro, R., et al. 2017, Sci, 358, 911
Accardo, L., Aguilar, M., Aisa, D., et al. 2014, PhRvL, 113, 121101
Ackermann, M., Ajello, M., Allafort, A., et al. 2012, PhRvL, 108, 011103
Adriani, O., Akaike, Y., Asano, K., et al. 2018, PhRvL, 120, 261102
Adriani, O., Barbarino, G. C., Bazilevskaya, G. A., et al. 2009, Natur, 458, 607
Aguilar, M., Aisa, D., Alvino, A., et al. 2014, PhRvL, 113, 121102
Aguilar, M., Ali Cavasonza, L., Ambrosi, G., et al. 2019, PhRvL, 122, 041102
Aharonian, F., Akhperjanian, A. G., Anton, G., et al. 2009, A&A, 508, 561
Aharonian, F., Akhperjanian, A. G., Barres de Almeida, U., et al. 2008, PhRvL, 101, 261104
Amato, E., & Arons, J. 2006, ApJ, 653, 325
Arons, J. 2012, SSRv, 173, 341
Atoyan, A. M., Aharonian, F. A., & Völk, H. J. 1995, PhRvD, 52, 3265
Barkov, M. V., Lyutikov, M., & Khangulyan, D. 2019, MNRAS, 484, 4760
Bergström, L., Bringmann, T., & Edsjö, J. 2008, PhRvD, 78, 103520
Bertone, G., Hooper, D., & Silk, J. 2005, PhR, 405, 279
Blasi, P., & Amato, E. 2011, in ASSP Proc. First Session of the Sant Cugat Forum on Astrophysics, High-Energy Emission from Pulsars and their Systems, 21 (Berlin: Springer), 624
Bogdanov, S. 2017, Modelling Pulsar Wind Nebulae, Astrophysics and Space Science Library Vol. 446 (Dordrecht: Springer), 295
Brownsberger, S., & Romani, R. W. 2014, ApJ, 784, 154
Büsching, I., Venter, C., & de Jager, O. C. 2008, AdSpR, 42, 497
Bykov, A. M., Amato, E., Petrov, A. E., Krassilchtchikov, A. M., & Levenfish, K. P. 2017, SSRv, 207, 235
Candia, J., & Roulet, E. 2004, JCAP, 10, 007
Casse, F., Lemoine, M., & Pelletier, G. 2002, PhRvD, 65, 023002
Cholis, I., Karwal, T., & Kamionkowski, M. 2018, PhRvD, 97, 123011
Crusius, A., & Schlickeiser, R. 1986, A&A, 164, L16
DAMPE Collaboration 2017, Natur, 552, 63
Della Torre, S., Gervasi, M., Rancoita, P. G., Rozza, D., & Treves, A. 2015, JHEAp, 8, 27
Evoli, C., Linden, T., & Morlino, G. 2018, PhRvD, 98, 063017
Fang, K., Bi, X.-J., Yin, P.-F., & Yuan, Q. 2018, ApJ, 863, 30
Frisch, P. C., Berdyugin, A., Piirola, V., et al. 2015, ApJ, 814, 112
Hooper, D., Blasi, P., & Serpico, P. D. 2009, JCAP, 1, 025
Hooper, D., & Linden, T. 2018, PhRvD, 98, 043005
Kargaltsev, O., & Pavlov, G. G. 2008, in AIP Conf. Ser. 983, 40 Years of Pulsars: Millisecond Pulsars, Magnetars and More, ed. C. Bassa et al. (Melville, NY: AIP), 171
Kargaltsev, O., Pavlov, G. G., Klingler, N., & Rangelov, B. 2017, JPlPh, 83, 635830501
Kisaka, S., & Kawanaka, N. 2012, MNRAS, 421, 3543
Kotera, K., Amato, E., & Blasi, P. 2015, JCAP, 8, 026
Lemoine, M., Kotera, K., & Pétri, J. 2015, JCAP, 7, 016
López-Coto, R., Hahn, J., BenZvi, S., et al. 2018a, APh, 102, 1
López-Coto, R., Parsons, R. D., Hinton, J. A., & Giacinti, G. 2018b, PhRvL, 121, 251106
Malkov, M. A., Diamond, P. H., Sagdeev, R. Z., Aharonian, F. A., & Moskalenko, I. V. 2013, ApJ, 768, 73
Malyshev, D., Cholis, I., & Gelfand, J. 2009, PhRvD, 80, 063005
Mignani, R. P., Pavlov, G. G., & Kargaltsev, O. 2010, ApJ, 720, 1635
Moderski, R., Sikora, M., Coppi, P. S., & Aharonian, F. 2005, MNRAS, 363, 954
Moskalenko, I. V., & Strong, A. W. 1998, ApJ, 493, 694
Olmi, B., & Bucciantini, N. 2019, MNRAS, 484, 5755
Posselt, B., Pavlov, G. G., Slane, P. O., et al. 2017, ApJ, 835, 66
Posselt, B., Spence, G., & Pavlov, G. G. 2015, ApJ, 811, 96
Profumo, S. 2012, CEJPh, 10, 1
Profumo, S., Reynoso-Cordova, J., Kaaz, N., & Silverman, M. 2018, PhRvD, 97, 123008
Rangelov, B., Pavlov, G. G., Kargaltsev, O., et al. 2016, ApJ, 831, 129
Reardon, D. J., Hobbs, G., Coles, W., et al. 2016, MNRAS, 455, 1751
Recchia, S., Gabici, S., Aharonian, F. A., & Vink, J. 2018, arXiv:1811.07551
Seta, A., Shukurov, A., Wood, T. S., Bushby, P. J., & Snodin, A. P. 2018, MNRAS, 473, 4544
Silk, J., & Srednicki, M. 1984, PhRvL, 53, 624
Strong, A. W., Moskalenko, I. V., & Ptuskin, V. S. 2007, ARNPS, 57, 285
Tang, X., & Piran, T. 2019, MNRAS, 484, 3491
Venter, C., Kopp, A., Harding, A. K., Gonthier, P. L., & Büsching, I. 2015, ApJ, 807, 130
Vladimirov, A. E., Jóhannesson, G., Moskalenko, I. V., & Porter, T. A. 2012, ApJ, 752, 68
Yüksel, H., Kistler, M. D., & Stanev, T. 2009, PhRvL, 103, 051101